6th European Conference on Computational Mechanics (ECCM 6)
7th European Conference on Computational Fluid Dynamics (ECFD 7)
11–15 June 2018, Glasgow, UK

STABILITY OF LOCAL OUT-OF-PLANE DEFORMATIONS OF ORTHOTROPIC SHEET: NUMERICAL APPROACH

ANNA-LEENA ERKKILÄ[1], TEEMU LEPPÄNEN[2] AND TERO TUOVINEN[1]

[1] University of Jyväskylä
PO Box 35, FI-40014 Jyväskylä, Finland
anna-leena.j.erkkila@jyu.fi, tero.tuovinen@jyu.fi

[2] LUT Savo Sustainable Technologies, Lappeenranta University of Technology, Varkaus unit
Opiskelijankatu 3, FI-78210 Varkaus, Finland
teemu.leppanen@lut.fi

Key words: Simulation, Finite Element Method, Structure, Heterogeneity, Stability, Out-of-plane Deformation

Abstract. Local variations in dimensional changes generate internal forces into material. These variations arise, for example, from material heterogeneity or from an uneven thermal or moisture field. Internal forces can cause different in-plane compressive forces as well as out-of-plane bending moments. This means that, in the case of a plate or sheet, both the buckling and bending type of out-of-plane deformation tendencies may occur. Buckling and nonlinear geometry may cause challenges in the reliable numerical prediction of the out-of-plane response. Finite element analysis is performed for an experimental plate structure using the orthotropic hygro-elasto-plastic model. Two aspects related to the simulated out-of-plane deformations are considered: the influence of boundary conditions and the effect of the sheet size and shape on stability. The results show the importance of the boundary conditions when cockling is compared to a production machine sample and highlight the strength of the structural variation to cause local bending, thus stabilizing the solution.

1 INTRODUCTION

Out-of-plane deformation of a paper sheet or board product is an undesired phenomenon induced by inhomogeneity in dimensional changes. Inhomogeneity may arise from variations in the structure, composition and moisture content or from uneven mechanical handling in any paper process or end use stage. The sorptive nature of paper fibers together with the elasto-visco-plastic material characteristics of paper implies the dynamic time- and history-dependent formation of out-of-plane deformations. The appearances of out-of-plane deformations are classified into several categories, e.g., curl, cockling and baggy paper webs. Curl, caused by differences in dimensions of the two sides of a sheet, can be detected as a deviation of the sheet edges from the flat position.

In the ideal case, curl can be considered to reflect the overall, usually cylindrical, shape of the paper sheet. The bagginess of a paper web can be detected as buckled or wave-like regions caused by strain streakiness of the web. The model presented in [1] and utilized for studies on curling and baggy web behavior in [1, 2] is used in this study for cockling prediction.

The cockling of a paper sheet becomes visible under inclined illumination showing the fluctuation of reflective and shadowy areas. This shading estimates the gradients of the sheet surface topography. The small-scale high gradients represent structures that are visually disturbing and regarded as cockling. The nature of cockling can vary significantly and it may counteract other out-of-plane behaviors e.g. with curl. Research on the cockling phenomenon was started in the 1950s by Smith [3], and only in the past few decades have a limited number of numerical studies concerning cockling been performed; see [4, 5, 6, 7, 8]. This paper employs numerical simulations to predict cockling caused by fiber orientation variations in paper sheets. The simulated cockling is compared to the measured topography of the sheet, and the stability of the local out-of-plane deformations is studied with different boundary conditions and sample sizes.

2 MEASUREMENTS

The studied sample is a production machine-made newspaper sheet taken from the middle of the paper web. The sample was produced from 100% deinked pulp with the basis weight of 45 g/m^2 and the thickness of 0.06 mm. In the cockling measurements, the topography was measured from the sheet conditioned under standard atmospheric conditions (RH = 50% +/- 2%, T = 23 °C +/- 1 °C) and then again from the same region of the sheet after a humidity treatment cycle. In the humidity cycle, the sample was conditioned at RH 88% at least 8 hours and then again at RH 50% at least 8 hours or until the sample reaches an equilibrium before the topography measurement. The topography of the out-of-plane deformations of the sheet was reconstructed from images captured using four lightning directions by photometric stereo [9, 10]. The measured region was 192 mm × 192 mm.

The local fiber orientation distribution structures throughout the sheet thickness were determined from the scanned layer images [11, 12] and defined by the orientation angles θ (°) and the anisotropies ξ (-) [13]. The orientation angle θ describes the deviation of the main direction of the fiber orientation distribution from the machine direction (MD). Anisotropy ξ is a ratio of the main and the minor axis of the distribution, see Fig. 3. The same in-plane region (192 mm × 192 mm) as in the topography measurements was analyzed and the results were interpolated to 10 equally thick layers. Fig. 1 presents the topography and fiber orientation structure variation in layers 3 and 8 from a 30 mm × 30 mm region of the studied sample. Line segments are used to describe the local orientation of a 0.6 mm × 0.6 mm region. Fig. 3 presents the arrangement of layers: layer 1 and layer 10 correspond to the bottom surface (BS) and top surface (TS), respectively.

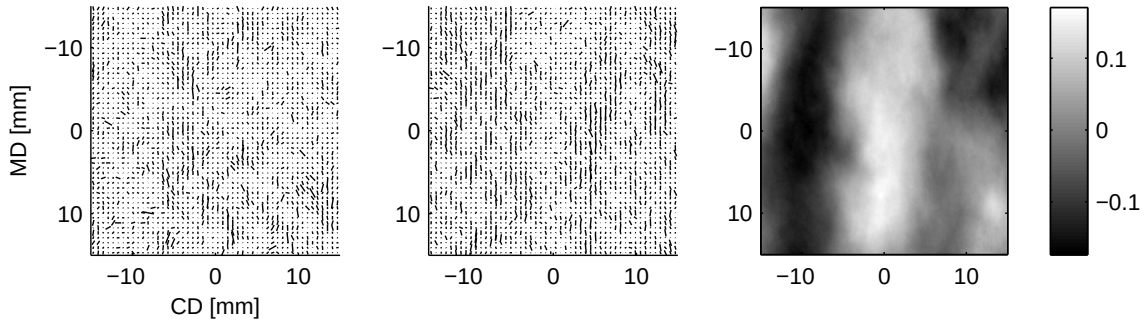

Figure 1: Fiber orientation of layers 3 (left) and 8 (middle) presented by line segments. Each line represents the fiber orientation in a 0.6 mm × 0.6 mm subregion in one layer. The length and the orientation of the segment describes the anisotropy (ξ) and orientation angle (θ) of the orientation, respectively. The image on the right shows a corresponding measured topography. The scale is in millimeters.

3 MATERIAL MODELS

Elasto-plastic material and hygroscopic shrinkage models were used to predict the out-of-plane deformation behavior of a paper sheet. An orthotropic material in the plane stress state was assumed. In the elasto-plastic approach, the dependence between stress $\sigma = (\sigma_1, \sigma_2, \sigma_{12})^\top$ and strain $\varepsilon = (\varepsilon_1, \varepsilon_2, \varepsilon_{12})^\top$ was defined by the generalized Hooke's law as

$$\sigma = C\left(\varepsilon - \beta \Delta c\right), \tag{1}$$

where C is the constitutive matrix, $\beta = (\beta_1, \beta_2, 0)^\top$ (%/%) is the moisture expansion coefficient and Δc (-) is the dry solids content (DSC) change. The direction 1 coincides with the orientation angle and the direction 2 is perpendicular to the direction 1. The non-linear dependence of material parameters on the anisotropy and dry solids content based on experimental results are derived in detail in the references [1] and [14]. Isotropic hardening was assumed and Hill's yield function was used to describe the yield surface. Fig. 2 displays examples of the simulated stress-strain curves.

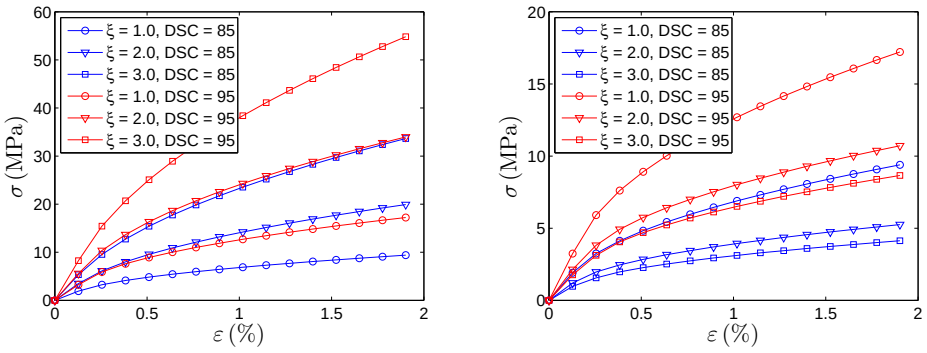

Figure 2: Stress-strain curves in the direction 1 (left) and the direction 2 (right) for the anisotropies ξ of 1, 2 and 3 with the dry solids contents (DSC) of 85% and 95%.

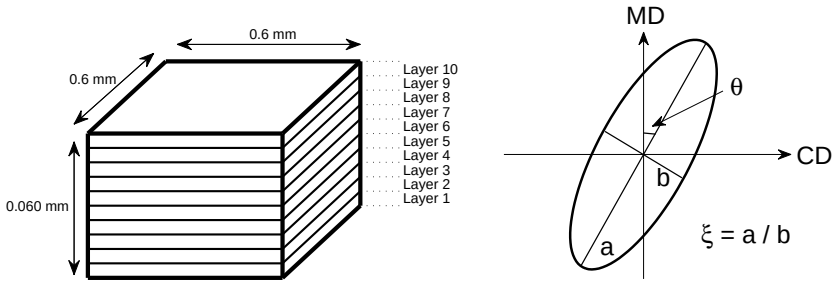

Figure 3: Layered structure of the element (left) and fiber orientation distribution defining the orientation of each layer (right).

4 SIMULATIONS

Numerical solutions were obtained with the finite element method (FEM). The simulations employed the commercial software Abaqus/Standard and its shell element S4R with a composite structure; see [15]. In the thickness direction which corresponds to the z-direction (normal of the MD-CD-plane, see Fig. 4) in the initial configuration, the elements were divided into 10 layers with equal thicknesses; Fig. 3 shows the element size and thickness of the simulated samples. Geometrical nonlinearity was assumed in the simulations. Automatic incrementation control and volume-proportional damping with the damping factor 10^{-8} were utilized to obtain the numerical solutions [15].

The in-plane layouts of the samples include five squares and eight rectangles. Fig. 4 shows the dimensions of the squares. The measured sample corresponds to the largest square with in-plane dimensions 192 mm × 192 mm from which the structures of the

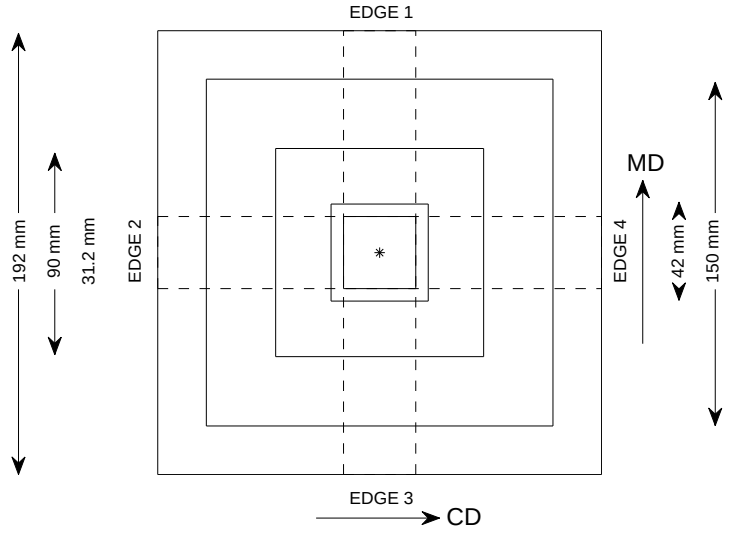

Figure 4: The layouts of the simulated samples include five squares and eight rectangles. The in-plane directions are defined by the paper making process as the machine direction (MD) and cross direction (CD). The middle point (MP) is marked with an asterisk and the node set containing all nodes of the sample is called ALL.

Table 1: Dry solids contents in the layers 1–10 at the end of the step 1. Fig. 3 presents the layer numbers.

	1	2	3	4	5	6	7	8	9	10
SP1–SP9	95	95	95	95	95	95	95	95	95	95
SP10	84	86	88	90	92	94	95	95	95	95
SP11,SP12,SP13,SP14	90.05	90.95	91.85	92.75	93.65	94.55	95	95	95	95

smaller samples were cut. Fig. 4 displays two rectangles as an example; similarly in the other six rectangles the longer dimension is always 192 mm, but the shorter edges take dimensions of the different square samples.

The simulation procedure SP1 was performed for all samples whereas the simulation procedures SP2–SP14 were performed for the sample with dimensions 150 mm × 150 mm. The simulation procedures SP1, SP7 and SP8 consisted of one step, SP2–SP6 and SP9 consisted of two steps and SP10–SP14 consisted of three steps. In all procedures, the initial dry solids content in all layers was 70 %. Table 1 presents the dry solids contents at the end of step 1. In the case of SP10–SP14, the constant dry solids content 95 % was achieved at the end of the step 2. Tables 2 and 3 shows the boundary conditions during the dry solids content change and during the final step, respectively. In addition, Table 3 shows that the in-plane displacements are always unrestrained at the end of the simulations.

5 RESULTS

Fig. 5 illustrates the measured out-of-plane deformations (before and after humidity cycling) and the prediction with the simulation procedure SP1. The correlation coefficient is used to evaluate the similarity of out-of-plane deformation shapes; the amplitude of cockling depends several factors, e.g. the ambient humidity and temperature, and is not relevant in this study. For the whole studied region (192 mm × 192 mm), the corre-

Table 2: Restrained degrees of freedom during the dry solids content change. Fig. 4 defines the edge numbers (1–4), the middle point MP and the node set ALL.

	u_{MD}	u_{CD}	u_z	ϕ_{MD}	ϕ_{CD}	ϕ_z
SP1,SP9,SP10,SP11	MP	MP	1,2,3,4,MP	2,4,MP	1,3,MP	MP
SP2,SP12	1,3,MP	2,4,MP	1,2,3,4,MP	2,4,MP	1,3,MP	MP
SP3,SP13	1,3,MP	MP	1,2,3,4,MP	2,4,MP	1,3,MP	MP
SP4,SP14	MP	2,4,MP	1,2,3,4,MP	2,4,MP	1,3,MP	MP
SP5	MP	MP	ALL	2,4,MP	1,3,MP	MP
SP6	ALL	ALL	ALL	2,4,MP	1,3,MP	MP
SP7	MP	MP	1,2,3,4	MP	MP	MP
SP8	MP	MP	1,2,3,4	2,4,MP	1,3,MP	MP

Table 3: Restrained degrees of freedom during the final step. Fig. 4 defines the edge numbers (1–4) and the middle point MP.

	u_{MD}	u_{CD}	u_z	ϕ_{MD}	ϕ_{CD}	ϕ_z
SP1–SP6	MP	MP	1,2,3,4,MP	2,4,MP	1,3,MP	MP
SP7	MP	MP	1,2,3,4	MP	MP	MP
SP8	MP	MP	1,2,3,4	2,4,MP	1,3,MP	MP
SP9–SP14	MP	MP	MP	MP	MP	MP

lations are 0.701 between the measured samples before and after humidity cycling, 0.439 between the measured before humidity cycling and simulated (SP1), and 0.470 between the measured after humidity cycling and simulated (SP1). Local correlations for areas of 30 mm × 30 mm are determined in every position of the sheet and presented in Fig. 5. The humidity cycling increases the amplitude of the measured cockling significantly. The shape of cockles remains mainly unchanged, but there are also diverging regions. The simulated out-of-plane deformations based on the fiber orientation structure predict local variations well for the most part but there are also some weak positions. Low correlation regions are not always in equivalent positions if the simulated result is compared with different measuring situations. Conditioning, history and handling have a significant effect

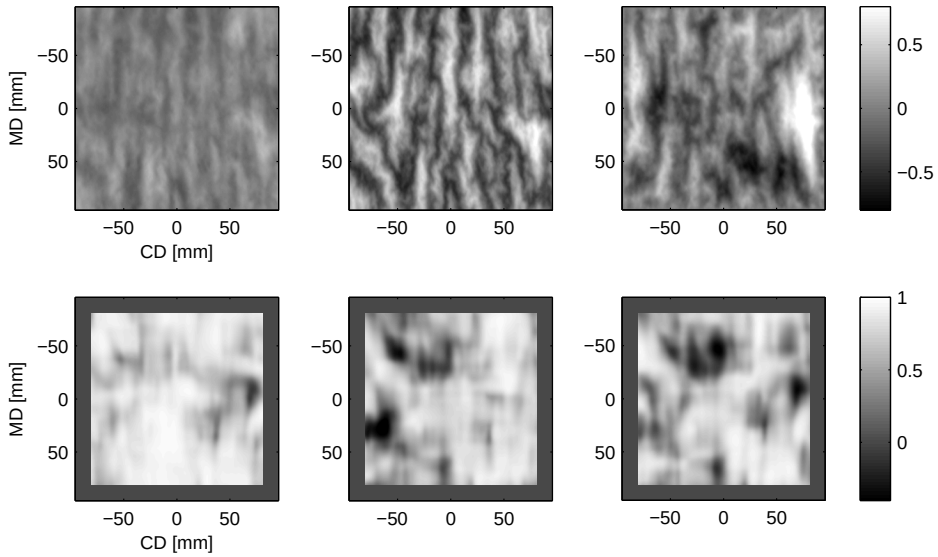

Figure 5: Top row (scale in millimeters): measured out-of-plane deformation before (left) and after (middle) humidity cycling. Simulated out-of-plane deformation with simulation procedure SP1 (right). Bottom row (scale corresponds to correlation coefficient): local correlation between the measured out-of-plane deformations (left), between the measured out-of-plane deformation before the humidity cycling and out-of-plane deformation of SP1 (middle), and between the measured out-of-plane deformation after the humidity cycling and out-of-plane deformation of SP1 (right).

on the cockling of a sheet. In addition, other factors besides fiber orientation variation have an effect on cockling.

Even fairly minimal differences in the anisotropy between the two sides of the sample create a curling tendency in the sheet. In the paper production process, the dry solids content differences in the thickness direction of the sheet, the prevention of in-plane shrinkage, and other restraints control curl. The studied sample has a fairly low fiber orientation based curl tendency, which is revealed using the simulation procedure SP9; see Fig. 6. The curl can be adjusted using a thickness directional drying profile in simulations as is demonstrated with SP10 and SP11. Although the curl is almost eliminated by the drying profile used in simulation procedure SP11, the equivalent drying profile does not guarantee that curl remains diminished when different in-plane straining is used, as in SP12, SP13 and SP14, i.e. the curl is very sensitive to boundary conditions and even the main axis of the curl may alter, as with simulation procedure SP14. Even minor curl has a high amplitude compared with cockling if the sheet size is larger than the cockling size scale. That is why filtering out the curl component, if there is any, is necessary if cockling is wished to be studied. To filter curl out of the simulated result, the 2D polynomial was fitted to an out-of-plane deformation surface and then subtracted from it. Fig. 6 presents the filtered predictions of simulation procedures SP9, SP11 and SP13 marked with an asterisk, and Fig. 7 shows their correlations with the measured samples. The correlations of the filtered topographies in the best cases (SP9*, SP11* and SP13*) are of the same

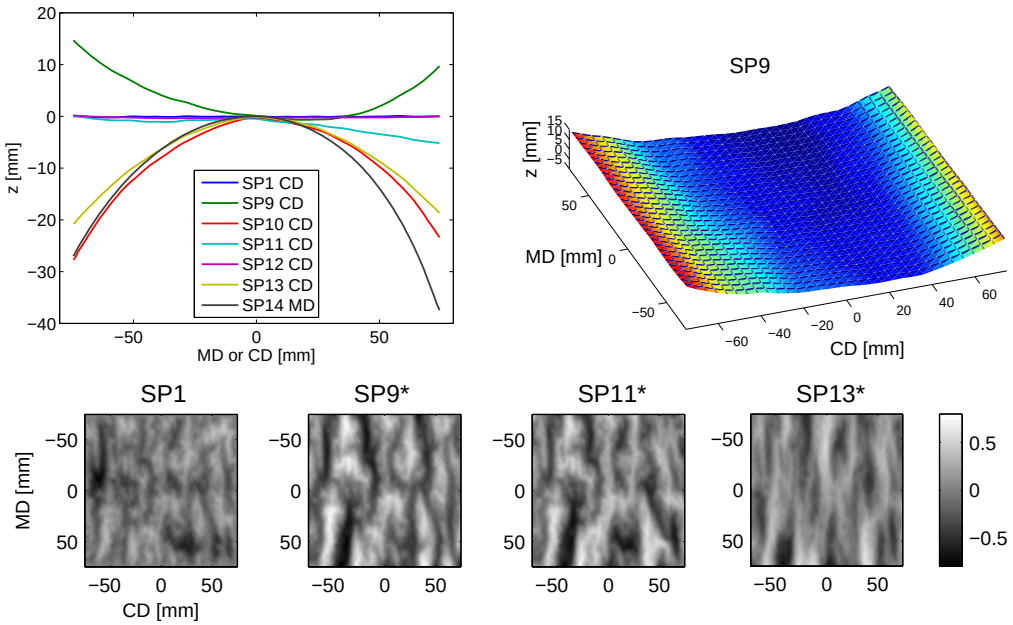

Figure 6: Sample size 150 mm × 150 mm. Top left: average MD or CD profiles derived from out-of-plane deformations predicted using different simulation procedures. Top right: simulated out-of-plane deformation with simulation procedure SP9. Bottom row: simulated cockling predictions; the asterisk expresses that curl has been filtered from the simulated out-of-plane deformation. The scale is in millimeters.

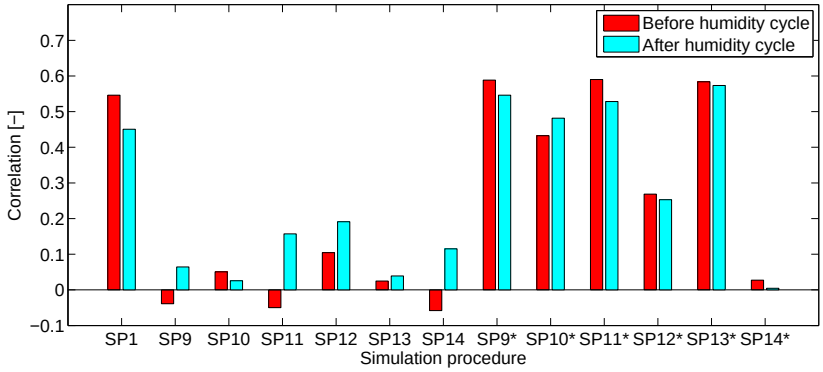

Figure 7: Sample size 150 mm × 150 mm. Correlations between the measured out-of-plane deformations and simulated results (SP1, SP9–SP14). The asterisk expresses that curl has been filtered from the simulated out-of-plane deformation.

order as with SP1. A visual observation of the topography of SP1 reveals that the small-scale cockles are more emphasized than in samples that are allowed to curl (Fig. 6). Curl suppresses some cockling, but releasing z-directional restraints at the edges improves the correlation of filtered out-of-planed deformations with measured ones. The reason for more notable improvement in the measured topography after humidity cycling than before cycling is that a paper sheet is more free to deform in humidity cycling compared to drying conditions during the paper manufacturing process. However, the simulations are significantly more time consuming in SP9–SP14, where z-directional boundary conditions of the edges are released in final step, than in SP1 where the restraints at the edges prevail. In the following, the edges are restrained in the z-direction in the final stage.

The effects of different combinations of restraints have been studied in SP1–SP8. Fig. 8 visualizes the out-of-plane results and Figs. 9 and 10 present the correlations between the measured and simulated out-of-plane deformations. MD restraints on edges 1 and 3 of the SP3 improve correlation because in the paper making process the sheet is restrained and even strained in MD. When CD restraints on edges 2 and 4 are applied in SP2, SP4 and SP6, the nature of cockling changes and correlations with measured results decrease clearly compared with SP1 and SP3. The z-directional restraints in SP5 and SP6 also show low correlations. Unrestrained rotations at the edges and an unrestrained z-direction in the MP at the final stage in SP7 have an effect on large-scale shapes of out-of-plane deformations. The unrestrained z-direction in the MP in SP8 is the only difference in boundary conditions compared to SP1; SP8 shows only a small decrease in the correlations compared to SP1. The boundary conditions have a significant effect on cockling shapes caused by local variations of stresses and strains arising from fiber orientation variation. However, the results prove that there is a clear correlation between measured and simulated cockling if the boundary conditions are appropriate; i.e. they imitate the restraints in the paper making process closely enough.

In Fig. 11, the effect of sheet dimensions on the stability of cockling results is studied when the size and shape of the modeled sheet varies. The simulation procedure SP1 is

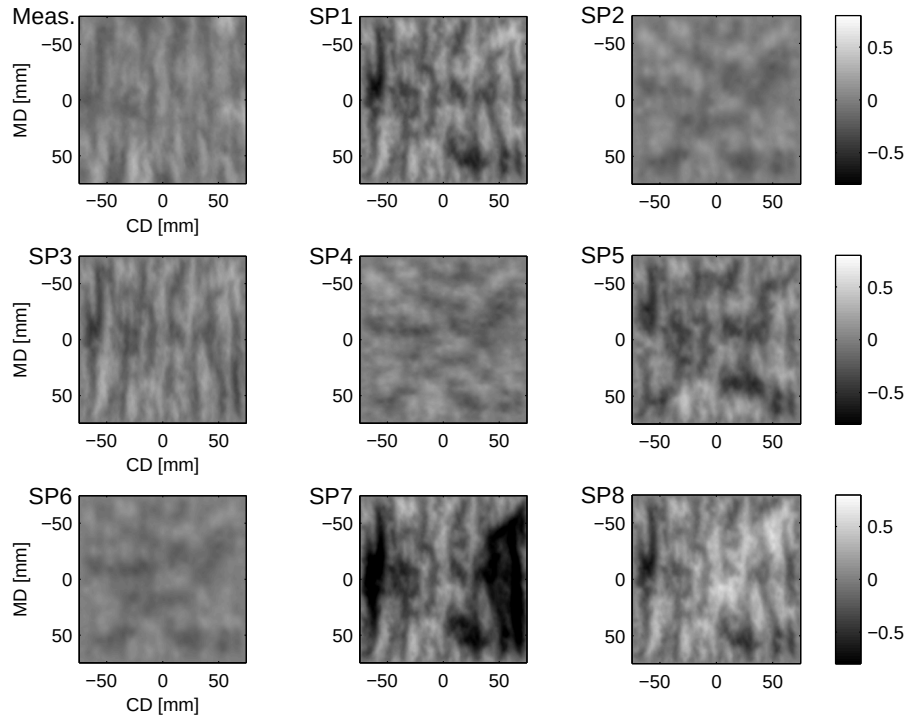

Figure 8: Sample size 150 mm × 150 mm. Measured out-of-plane deformation before humidity cycling (top left) and simulated out-of-plane deformations with simulation procedures SP1–SP8. The scale is in millimeters.

used. Overall, the differences between simulated topographies of square sheets of different sizes are minor. Wave-like differences on the edges and some local areas sensitive to buckling can be noticed. The waviness in MD and CD strips is mainly observed on the longer edges of the sheet, but also some large-scale differences are apparent in next to the short edges. The most significant differences arise in narrow CD strips. Strips display buckling similar to those of square sheets; their size and locations are equivalent,

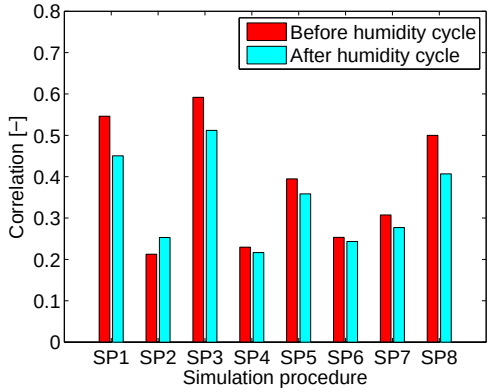

Figure 9: Sample size 150 mm × 150 mm. Correlations between the measured out-of-plane deformations and simulated results with simulation procedures SP1–SP8.

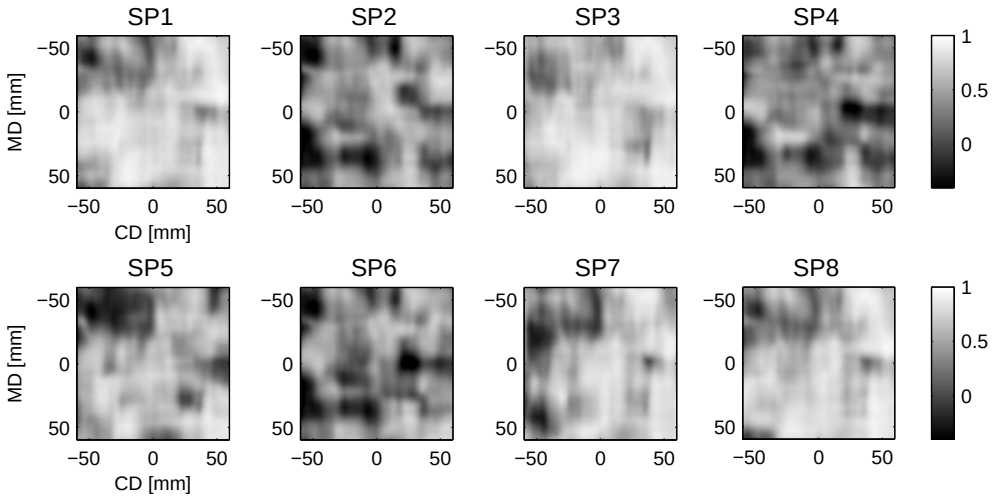

Figure 10: Local correlations between the measured out-of-plane deformation before humidity cycling and simulated out-of-plane deformations (SP1–SP8)

indicating that there are locations where measured fiber orientation structure enables bifurcation.

6 CONCLUSIONS

The out-of-plane deformations are simulated using measured fiber orientation variation as a source of variations in local material properties and moisture based shrinkage tendency. The boundary conditions have a significant effect on out-of-plane deformations, their overall shapes, such as curl and baggy, but also on cockling shapes. There is, however, a clear correlation between measured and simulated cockling with the few different simulation procedures and boundary condition choices. It can be assumed that a good correlation between a measured and simulated result is achieved if the boundary conditions of the simulation imitate the restraints in the paper making process closely enough. Although the fiber orientation can usually determine the direction of local cockle via local bending moments, there are a few positions where buckling takes place. Large-scale out-of-plane deformations, such as curl, increase the time consumption of simulations via nonlinear deformation and interfere with cockling. With the simulation procedure where the edges are restrained in the z-direction to prevent curl, the size and shape of the sheet mainly only affect the edges except in very narrow strips.

7 ACKNOWLEDGEMENTS

The simulations were performed with the commercial software Abaqus, which was licensed to CSC (the Finnish IT Center for Science).

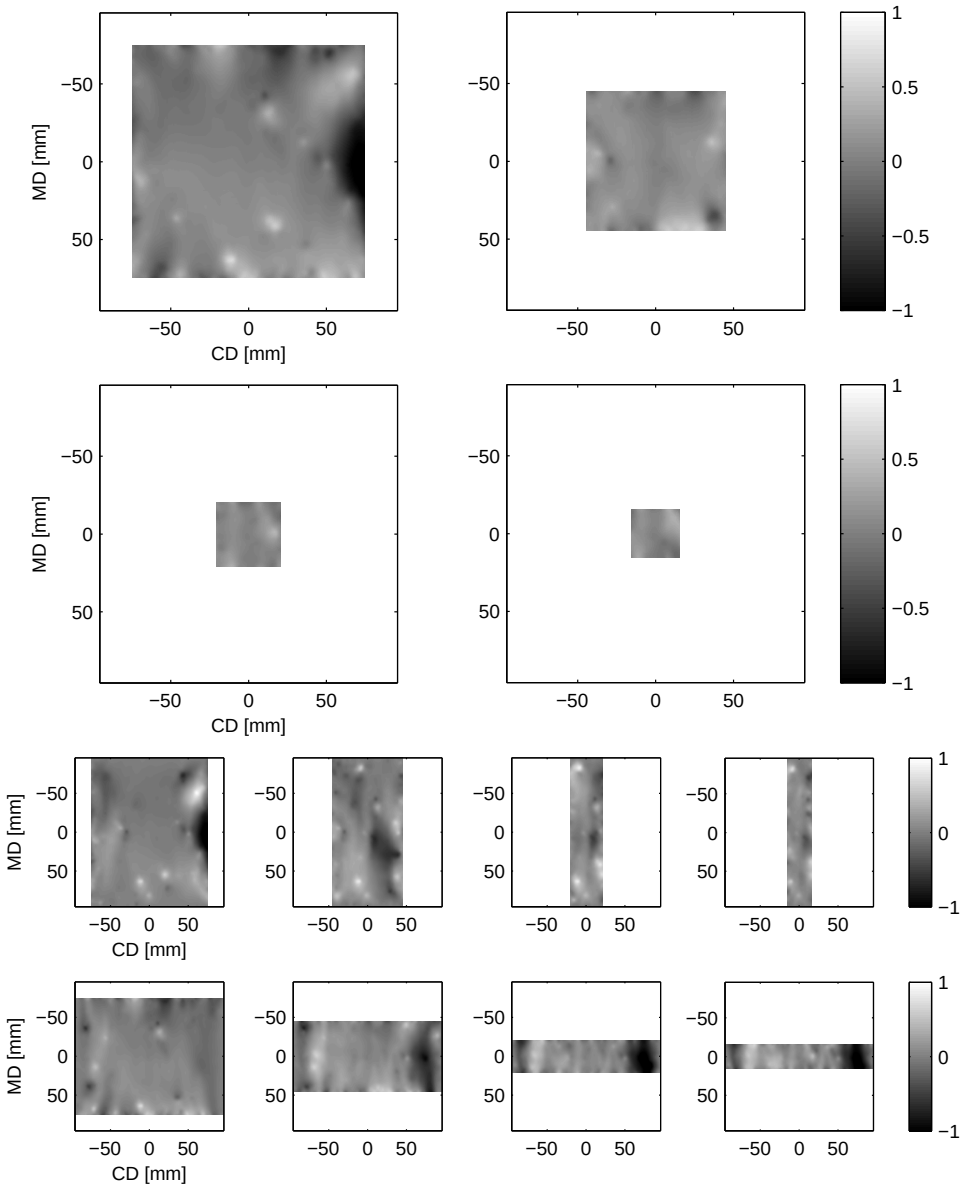

Figure 11: Differences between the simulated out-of-plane deformations (simulation procedure SP1) when compared to the size 192 mm × 192 mm. Scale is in millimeters. Dimensions of the samples are presented in Fig. 4.

REFERENCES

[1] Erkkilä, A.-L., Leppänen, T., Hämäläinen, J. and Tuovinen, T. Hygro-elasto-plastic model for planar orthotropic material. *International Journal of Solids and Structures* (2015) **62**:66-80.

[2] Erkkilä, A.-L., Leppänen, T. and Tuovinen, T. The curl and fluting of paper: the effect of elasto-plasticity. *Proceedings of the VII European Congress on Computational Methods in Applied Sciences and Engineering*, pp. 4752-4769, Crete, Greece, 2016.

[3] Smith, S.F. Dried-in strains in paper sheets and their relation to curling, cockling and other phenomena. *The Paper-Maker and British Paper Trade Journal* (1950) **119**:185-192.

[4] Leppänen, T., Sorvari, J., Erkkilä, A.-L. and Hämäläinen, J. Mathematical modelling of moisture induced out-of-plane deformation of a paper sheet. *Modelling and Simulation in Materials Science and Engineering* (2005) **13**:841-850.

[5] Leppänen, T. and Hämäläinen, J. Effect of local curls on the cockling of paper. *Nordic Pulp and Paper Research Journal* (2007) **22**:72-75.

[6] Kulachenko, A. and Uesaka, T. The effects of fibre orientation streaks on out-of-plane instability of paper. *Proceedings of the 2007 International Paper Physics Conference*, pp. 255-260, Gold Coast, Australia, 2007.

[7] Lipponen, P., Erkkilä, A.-L., Leppänen, T. and Hämäläinen, J. On the importance of in-plane shrinkage and through-thickness moisture gradient during drying on cockling and curling phenomena. *Proceedings of the 14th Fundamental Research Symposium*, pp. 389-436, Oxford, UK, 2009.

[8] Könnö, J. and Stenberg, R. Finite element analysis of composite plates with an application to the paper cockling problem. *Finite Elements in Analysis and Design* (2010) **46**:265-272.

[9] Woodham, R.J. Gradient and curvature from photometric-stereo method including local confidence estimation. *Journal of Optical Society of America* (1994) **11**:3050-3068.

[10] Hansson, P. and Johansson, P.-E. A new method for the simultaneous measurement of surface topography and ink distribution on prints. *Nordic Pulp and Paper Research Journal* (1999) **14**:315-319.

[11] Erkkilä, A.-L., Pakarinen, P. and Odell, M. Sheet forming studies using layered orientation analysis. *Pulp and Paper Canada* (1998) **99**(1):81-85.

[12] Erkkilä, A.-L., Pakarinen, P. and Odell, M. The effect of forming mechanisms on layered fiber structure in roll and blade gap forming. *Proceedings of the TAPPI 99 - preparing for the next millennium*, pp. 389-400, Atlanta, USA, 1999.

[13] Erkkilä, A.-L. Hygro-elasto-plastic behavior of planar orthotropic material. *Acta Universitatis Lappeenrantaensis 631, Diss. Lappeenranta University of Technology*, Lappeenranta, Finland, 2015.

[14] Erkkilä, A.-L., Leppänen, T. and Hämäläinen, J. Empirical plasticity models applied for paper sheets having different anisotropy and dry solids content levels. *International Journal of Solids and Structures* (2013) **50**:2151-2179.

[15] *Abaqus documentation*, Dassault Systèmes, 2013.